STOCHASTIC TECHNIQUES FOR MODELLING BRAIN CONNECTIVITY IN NEUROIMAGING

Pedro Osório

Instituto Superior Técnico

ABSTRACT

A fundamental question in neuroscience is how different brain areas communicate with each other. Dynamic causal modelling (DCM) is a generic formalism to study effective brain connectivity based on neuroimaging data, particularly functional magnetic resonance imaging (fMRI). The interactions between neuronal activity at different brain areas areas are modelled as a first-order differential equation which also incorporates a generative model of how the neuronal activity is transformed into the measured haemodynamic fMRI response - the haemodynamic response function (HRF). The problem of discriminating between different structures of connectivity can be solved by state-of-the-art Bayesian methods, whereby parameter estimation is followed by model selection. These methods are computationally expensive and may converge to parameter values that are valid only for a particular dataset. In this thesis, the well-known multiple-model kalman filter (MMKF) is applied in a number of different ways to perform model selection in an efficient manner, upon simulated data from models with different connectivity structures. The problem of estimating the haemodynamic response function (HRF) is first addressed and the methodology is then extended to the full problem of estimating the DCM. The results show that the MMKF seems to be very accurate at choosing the correct connectivity structure between two parametrized models, even taking into account the output non-linearity (the HRF). In conclusion, this work provides the first demonstration of the applicability of MMKF approaches to the problem of estimating effective brain connectivity based on DCM for fMRI.

Index Terms— fMRI, Dynamic Causal Modelling, Multiple Model Estimation, Kalman Filter

1. INTRODUCTION

Brain connectivity is an ill-defined concept[1]. From early studies of brain anatomy [2], the anatomic point of view was the center of connectivity research in neuroscience, and still today the human brain connectivity is not completely mapped [3]. More recently, the concepts of functional connectivity, mathematical correlation between activity in different brain areas, and effective connectivity, which requires causality, have developed. The latter, in particular, has been the subject a good amount of work (and controversy) in the neuroimaging community in the last years[4].

There have been several approaches to modelling brain connectivity that differ in their choice of observation equation (how brain states translate to a measured signal) and the state equation that describes the evolution of the brain states with time. Notably, Granger causality mapping (GCM) as an example of a data-driven approach [5], and DCM as an example of a model-driven (biophysically inspired) one[6]. In this paper, the focus is on the DCM.

1.1. DCM

Dynamic causal modelling consists of a parsimonious model - a bilinear dynamical system - where the average *neuronal activity* is the state variable that represents each brain area, and can be described by the following equation:

$$\dot{z}(t) = (A + \sum_j u_j(t) B^{(j)}) z(t) + Cu(t) \qquad (1)$$

Here, z(t) is the vector of neuronal activity at different brain areas, and u(t) is the vector of all inputs at time t (the inputs are any known external stimuli that can influence brain activity, within a controlled experiment). **A** has negative terms on the diagonal (natural rate of decay of neuronal activity in each area) and the non-zero terms off-diagonal represent intrinsic communication between brain areas for the given task. Each **B** controls the influence the j-th input has on the connections between brain areas (for instance, when a subject is told to pay attention to stimuli, certain connections may be enhanced and others inhibited). Matrix **C** represents the direct influence of stimuli on each brain area.

The activity of each brain area cannot be directly observed, and a specific neuroimaging technique must be used to obtain measures which can be realted to it. The function that describes the measured output of the system as a function of the underlying neuronal activity is called the forward model (it explains how observations are synthesized from the underlying hidden neural activity, as opposed to the inverse model, which would produce the neural activity given the observed signal). In the case of fMRI, that is the HRF.

1.2. Estimating Effective Brain Connectivity with DCM

Estimating effective brain connectivity with DCM requires the estimation of which models are superior to others in explaining the data. This usually involves inversion of the model. For this reason, techniques that deal with the inversion of the observation model (the HRF), are important. Apart from the one by Friston [7], alternatives have been proposed based on the extended Kalman filter [8], sequential Monte Carlo methods[9] and the unscented Kalman filter [10] as well as multiple-model Set-valued observer (SVO) [11].

Regarding the estimation of brain connectivity, the typical process based on DCM follows a two-step approach:

- A number of plausible models are proposed and the parameters of these models are estimated using a variational Bayes algorithm [12]. In the process, not only the neural connectivity but also the forward model parameters are estimated.
- These models are assessed using Bayesian model comparison (BMC), and the best one is chosen.

The equations that govern this scheme are:

$$\log p(y|m) = F(q) + D_{KL}(q(\theta) : p(\theta|y,m)) \quad (2)$$

$$F(q) = \langle log(p(\theta|m) + \log(p(y|\theta,m)\rangle_q + S(q) \quad (3)$$

In order to perform Bayesian model inversion, the priors for all parameters are defined and then they are estimated using Laplace approximation while maximizing F(q). Since the Kullback-Leibler divergence is nonnegative, F(q) is a lower-bound for the log-likelihood of the model. BMC uses these log-likelihoods to compare models. Since a lower-bound is used, the model comparison is not as reliable as it could be and this is admitted as a weakness of DCM by the authors [13].

1.3. Multiple-model kalman filter

Under measurement errors, typical state estimation techniques require the exact specification of the model parameters. When these are not available due to model uncertainty, it is not possible to build a state observer through classical estimation tools [14].

A solution which is more robust to parameter uncertainty is the multiple-model estimation [15]. Specifically for the case of estimating connectivity structure using DCM, given that the underlying biology is a lot more complex, it may just be that the neural model is too coarse resulting, among other things in a posterior distribution of the parameters that is clearly multi-modal. Since the standard DCM estimation approach tries to estimate the optimal parameters for a given connectivity structure by fitting a Gaussian distribution around the maximum of the free energy, if the true posterior distribution is actually multi-modal it may result in a loose lower bound of the model evidence and thus compromise the model comparison. If, on the other hand, one starts with the assumption that several parameter configurations may be correct, these issues may be obviated and thus allow for a more robust model selection in the context of effective connectivity estimation.

Instead of the standard fitting of one model, several models representative of the possible (parameter) states of the system can be used. The states of each of these models can be estimated by different types of observers, ranging from Kalman filters (KFs) [16] to SVOs[17].

For the reasons above, multiple-model estimation seems like a good idea for tackling the problem of identifying network connectivity in DCM. Given the choice between several multiple-model estimation algorithms, this thesis focuses on the MMKF [18][19], the multiple-model counterpart of KF, a very well studied filter, known to be the minimum variance unbiased estimator for linear systems, which has also been applied (with modifications) extensively as a non-optimal filter to non-linear systems.

An interesting point about the MMKF is that despite being primarily a tool for state estimation, it inherently performs model selection (through the probability distribution over the set of models).

Explicitly, for an MMKF with n models - $\mathcal{H}_1 \cdots \mathcal{H}_n$ - if the full data up to time k is defined as:

$$Y[k] \equiv \{u[0] \cdots u[k-1], y[1] \cdots y[k]\} \quad (4)$$

The prior probability over the models must be defined (typically a uniform distribution, if there's no reason to believe that some regions of the parameter space are more relevant a priori). All that is needed is a recursive formula that allows the computation of the probability of each model at time k+1 given the probabilities at time k:

$$P_i[k+1] = \frac{p(y[k+1]|\mathcal{H}_i, u[k], Y[k])}{Z} \cdot P_i[k] \quad (5)$$

(5) is a direct application of Bayes' rule and Z is a normalizing constant.

The fundamental assumption is that one of the models in the MMKF corresponds to the true model. In this case, the MMKF converges to the true model given a reasonable level of noise. However, even if the true model is not in the set considered in the MMKF (which will happen almost surely in a continuous parameter space), this approach still has its merits and it will converge almost surely to the model that is closest to the real system in terms of the measure defined by Baram[20].

1.4. Organization

In the next section, the methodology for applying MMKF to the selection of a HRF model is described and the results of

its application to simulation and empirical data are presented. After, the methodology is extended to the selection of DCM connectivity models and the results of simulation presented. In the last section, the final remarks and possible future work.

2. HAEMODYNAMIC RESPONSE FUNCTION ESTIMATION

The set of equations that comprise the HRF model is:

$$\dot{s} = \epsilon u - k_s s - k_f(f-1) \quad (6a)$$
$$\dot{f} = s \quad (6b)$$
$$\dot{v} = \frac{1}{\tau}(f - v^{\frac{1}{\alpha}}) \quad (6c)$$
$$\dot{q} = \frac{1}{\tau}\left(f\frac{1-(1-E_0)^{\frac{1}{f}}}{E_0} - v^{(\frac{1}{\alpha}-1)}q\right) \quad (6d)$$
$$y = V_0[k_1(1-q) + k_2(1-\frac{q}{v}) + k_3(1-v)] \quad (6e)$$

The HRF is the nonlinear dynamical system described by the equations above, and relating blood flow (f) with the blood oxygenation level dependent (BOLD) signal (y). Its state varibles are the volume (v) and deoxyhemoglobin content (q). Friston complemented this model by expressing the blood flow as a function of the synaptic activity (u), adding another state variable to the system: the flow-inducing signal (s). All of these except for the flow-inducing signal are normalized with respect to the resting state.

Estimating the parameters of the HRF is not trivial as it is a nonlinear system, with parameter identifiability issues (due to the number of parameters that need to be estimated from a single-input single-output (SISO) system). The low sensitivity of the output to local variation in the parameters has been previously shown[21] and justifies an approach, such as the MMKF, where the correct HRF is chosen from a set of models representative of the different physiologically plausible HRFs.

Given a set of different models, all described by (6), but with different parameter values, where the input to the system is assumed to be known (corresponding to the fMRI experiment design), the goal is to determine which one is the closest to the *true* HRF.

2.1. Methods

In order to accomplish this, the MMKF will be used with some modifications since the HRF is neither linear nor discrete in time. Hence, the required adjustments are:

- (Bi-)Linearization
- Discretization

2.1.1. Bilinearization

The bilinearization was first proposed in[7], the same paper that formulated the full model, and has been repeatedly used since then. Defining:

$$x = [s, f, v, q] \quad (7)$$
$$\dot{x} = F(x, \theta, u) \quad (8)$$
$$y = \lambda(x) \quad (9)$$

The bilinear approximation to the function F can be found by using Taylor's formula around $x = x^*$ and $u = 0$. After performing a variable change in x, a matrix formula can be obtained:

$$\tilde{x} \equiv [1\ x]^T \quad (10)$$
$$\dot{\tilde{x}} = A\tilde{x} + uB\tilde{x} = (A + uB)\tilde{x} \quad (11)$$

One must not forget that (6e), the output, is also nonlinear. Since the final system may be time-varying, as the MMKF allows it, its linearization proceeds in a straightforward fashion:

$$y = \underbrace{\left[\lambda(x) + \frac{\partial\lambda(x)}{\partial x}\cdot x \quad \frac{\partial\lambda(x)}{\partial x}\right]}_{C}\cdot\tilde{x} \quad (12)$$

The equations (11) and (12) constitute a linear continuous time-varying (LCTV) system, because A, B, C and u depend on time, and it is now a step closer to being suitable for MMKF treatment.

2.1.2. Discretization

Perhaps more important than the linearization of the model is the discretization, as this step is required to implement any model in a digital computer. After a discretization period ΔT is chosen, it is assumed that the continuous time-varying matrices and the input remain constant during this sampling interval:

$$A[k] = A(t) + B(t)u(t), t \in [k\Delta T, k\Delta T + \Delta T[\quad \forall k \quad (13)$$

One can then integrate (11) during this discretization step, to obtain:

$$\tilde{x}(k\Delta T + \Delta T) = \underbrace{e^{A[k]\cdot\Delta T}}_{\tilde{A}[k]}\tilde{x}(k\Delta T) \quad (14)$$
$$\tilde{x}[k+1] = \tilde{A}[k]\tilde{x}[k] \quad (15)$$

The continuous output equation (12) can be directly discretized:

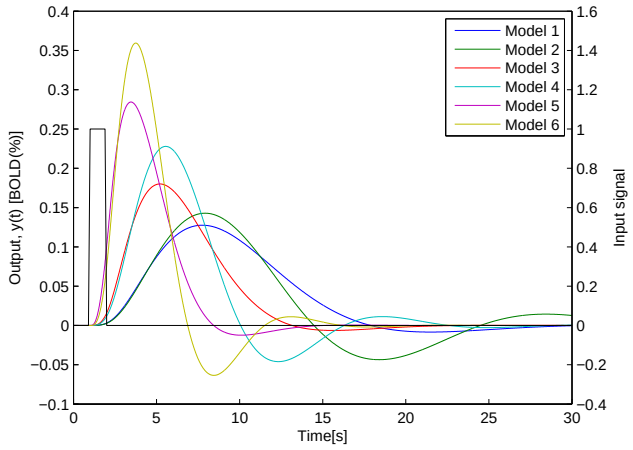

Fig. 1. The output of 6 different haemodynamic response functions to a unitary input

$$C[k] = \left[\lambda(x[k]) + \frac{\partial\lambda(x[k])}{\partial x} \cdot x[k] \quad \frac{\partial\lambda(x[k])}{\partial x}\right] \tag{16}$$

$$y[k] = C[k]\tilde{x}[k] \tag{17}$$

It can be seen that (15) and (17) fit perfectly into the linear discrete time-varying (LDTV) framework required by the KF, and are thus finally in a form that allows the use of MMKF.

2.1.3. Parameters

A set of 6 physiologically plausible HRF models are used that display the stereotypical known features of the HRF, specifically: fast, medium or slow response with or without undershoot. The parameters of these models are in the table 1.

HRF	k_s	k_f	τ	α	E_0
1	$0.400\ s^{-1}$	$0.100\ s^{-1}$	$2.080\ s$	0.320	0.340
2	$0.220\ s^{-1}$	$0.110\ s^{-1}$	$2.180\ s$	0.320	0.340
3	$0.650\ s^{-1}$	$0.200\ s^{-1}$	$0.880\ s$	0.320	0.340
4	$0.450\ s^{-1}$	$0.300\ s^{-1}$	$1.580\ s$	0.320	0.340
5	$0.950\ s^{-1}$	$0.450\ s^{-1}$	$0.200\ s$	0.320	0.340
6	$0.750\ s^{-1}$	$0.600\ s^{-1}$	$0.500\ s$	0.320	0.340

Table 1. Biophysical parameters for the 6 HRF models considered.

For each of the models, the neuronal efficacy ϵ is determined depending on the experimental data (input design and observed BOLD response) by doing a binary search on the parameter ϵ, trying to minimize the absolute difference between a feature computed for the current model and the same feature computed on the observed response.

Typically, the BOLD response is obtained as a zero mean signal, although the haemodynamic model assumes the baseline to be 0 and most of the signal to be above that value. This means that the model so far presented would not fit the experimental data as it is. The approach here, consists in assuming that the zero mean signal must be shifted vertically, that is, an offset v_{off} must be added to the experimental data. In order to find the best value for a given model that has response y_i, we can just minimize the sum of squared errors.

The MMKF requires an estimate of the noise in the measurement model. In order to obtain this estimate, one of the HRFs is used to filter the input for a given experiment and the Fast Fourier Transform (FFT) [22] of the output is then computed. By finding the bins that contain the least amount of signal energy (up to 5% cumulatively), one can use these to detect the frequencies where an ouput signal from the same experiment is supposed to contain mostly noise and thus estimate the Signal to Noise Ratio (SNR) of other data, where the SNR is defined as:

$$SNR = \frac{\mu_{signal}}{\sigma_{signal}} \tag{18}$$

2.1.4. Simulations

Data were simulated using the parameters of the sixth model in table 1 and using as input signal 300s of a rectangular wave with period 8s and duty cycle of 50%. The integration step is 0.1s but the signal is sampled to get a simulated repetition time (TR) of 3s. These data were corrupted with band limited Gaussian noise with three levels of standard deviation to produce data with SNR of 1, 5 and 15. All preprocessing steps were performed as described above.

2.1.5. Empirical data

A set of empirical data from an fMRI experiment was used to test the model. Visual stimuli lasting 18s alternated with fixation periods with roughly the same duration, for a total of 366s, were used. The value of TR was 3s. After preprocessing of the raw signal, and performing the identification of an activated voxel on the visual cortex with the usual tools (general linear model (GLM)), its corresponding time-series, constisting of 122 points, was used as the experimental data (y) for the model selection procedure.

2.2. Results and Discussion

2.2.1. Simulations

Figure 2 displays the results of applying MMKF to the problem of HRF model selection when the correct model belongs to the set of tested models. The results clearly show that the selection is successful as model 6 is given a very high probability at the end of the data. As expected, higher SNR leads the method to converge faster (almost 100% after 50s

for SNR=15), but even for SNR=1, the system converges to a probability around 90% in less than 200s. Also worth noting is the fact that across all levels of SNR the second most likely model (though much less than the selected one) is consistently model 5. Inspecting figure 1 this seems natural as model 5 is the only other model to have a time-to-peak as short as the one featured by the correct model.

2.2.2. *Empirical data*

Figure 3 shows the evolution of the probability of each model and the fit of the best model, on the visual task empirical data. On the empirical data, it is harder to draw conclusions as the ground-truth is not available. However, model 3 is selected after processing only a fraction of the data.

One must bear in mind that with experimental data the correct model will never be in the set of models that the algorithm can choose from and this may lead to indefinition.

3. DYNAMIC CAUSAL MODEL ESTIMATION

The main goal of this chapter is to determine which brain areas have a effective connectivity during a certain task or which connections a certain stimulus modulates. This amounts to determining the structure of matrices **A** and **B**, that is, which off-diagonal terms are zero.

3.1. Methods

The MMKF will again be used to select between a number of models. This time taking into account the coupled system defined by (1) and (6).

As in the previous chapter, (1) must be adapted so as to fit into the MMKF. We start by obtaining a discrete-time model that describes the dynamics in (1).

Defining $F(t) = A + \sum_j u_j(t)B^{(j)}$, and assuming the inputs are continuous in the interval $t \in [k\Delta T, k\Delta T + \Delta T[\quad \forall k$, it is possible to integrate (1) at the sampling times on each of the intervals:

$$z(k\Delta T + \Delta T) = e^{F(k\Delta T)\cdot\Delta T} \cdot z(k\Delta T) + C(e^{F(k\Delta T)\cdot\Delta T} - I)F(k\Delta T)^{-1}u(k\Delta T) \quad (19)$$

$$z[k+1] = e^{F[k]\cdot T} z[k] \cdot z[k] + C(e^{F[k]\cdot T} - I)F[k]^{-1}u[k] \quad (20)$$

In order to apply the MMKF to the full system in one pass, the DCM and HRF are integrated into one augmented state vector, where (for a DCM with n brain areas) the first n entries correspond to the vector z and the state vectors for the HRF (each with 5 elements) are stacked below. The matrices of the dynamical system are assembled in a compatible way, thus completing the definition of the LDTV that a KF requires.

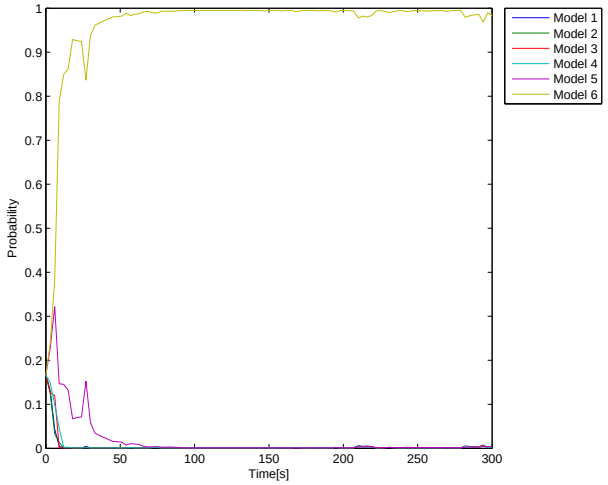

(a)

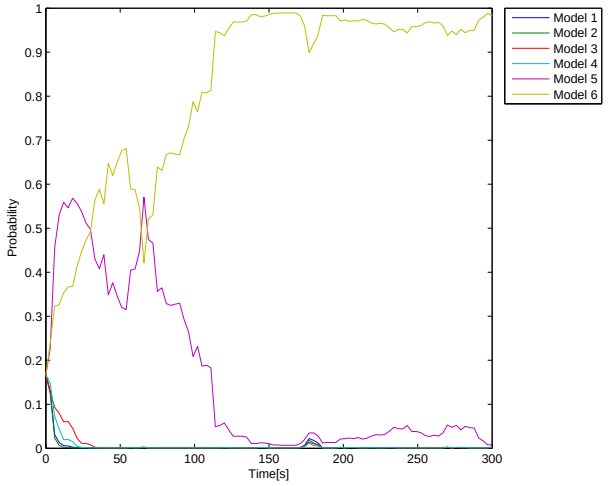

(b)

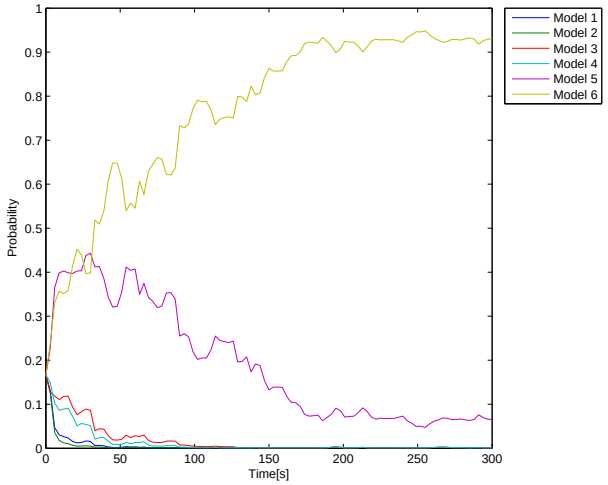

(c)

Fig. 2. Probability of the different haemodynamic models, when the simulated model is number 6 with (a) SNR=15 (b) SNR=5 (c) SNR=1

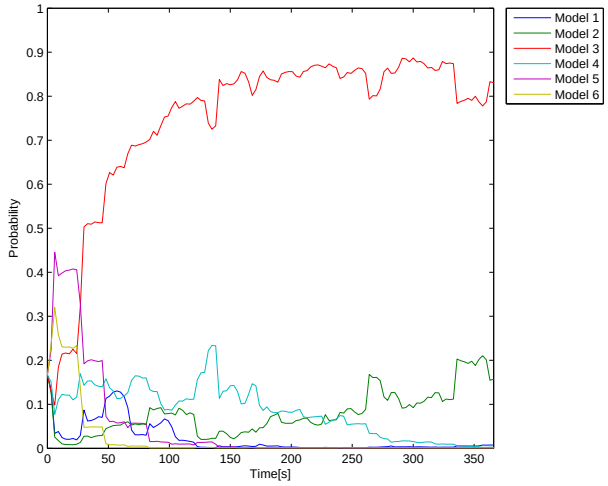

(a)

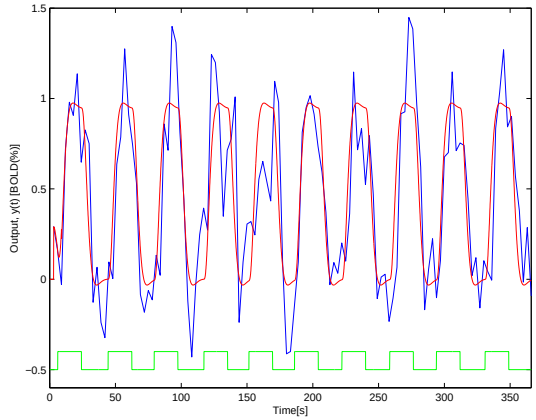

(b)

Fig. 3. Probability of the different haemodynamic models on the visual task (a) and best fit (b)

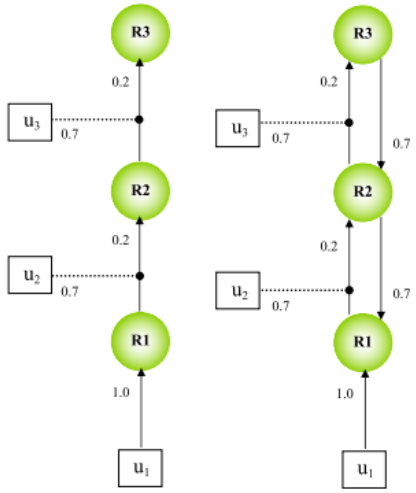

(a)

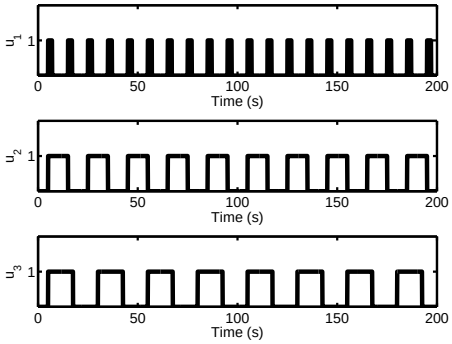

(b)

Fig. 4. Two models with different intrinsic connectivity (a) and inputs used in simulation (b)

3.1.1. Models and Parameters

In the following, the acMMKF is evaluated in the task of distinguishing between two models with different intrinsic connectivity structures from [23]. They can be seen in 4 as well as the inputs used in simulations.

Unless otherwise noted, a simulation from any model in these scenarios consists of 200s of data generated with an integration step of 0.1s and posterior subsampling to simulate TR=3s. For the estimation of the DCM structure, the HRF is assumed known and it corresponds to the fourth set of parameters in table 1. Gaussian white noise is added to the outputs to generate data with different SNRs. Unlike the HRF case, the SNR is not estimated but assumed known (i.e. possibly estimated from the signal in regions where there is no activity).

3.1.2. Known DCM Parameters

The first approach to gauge the performance of MMKF in estimating the underlying structure of a DCM is to generate data from each of the (parametrized) models, and have MMKF decide which one is the correct. 100 Monte-Carlo simulations are performed – in this case the output generated is always the same, each of the simulations only differs in the particular realization of the noise added, for all of them SNR ≈ 1.

This is the simplest case possible, since the only difficulty is the added noise. The nonlinearity (the HRF) is known and one of the models that the algorithm can pick is equal to the model that generated the data. For the known parameters, the results are presented as box plots.

3.1.3. Unknown parameters

The second approach consists of generating data, not from the exact model depicted in the figures above, but from a model

that has the same structure but random parameters in a given range. In this case, for each of the 500 Monte-Carlo runs, each connection parameter is sampled from a uniform distribution in the range [0.1 , 0.9], data generated with added noise (here three levels of noise are tested, SNR $\approx$ 0.25, SNR $\approx$ 1 and SNR $\approx$ 10) and then the MMKF had to decide between the two models. Each KF represented one of the models, with parameters as close to the mid-range (0.5) as possible, while ensuring stability. That is, with maximum input, the eigenvalues of the matrix that multiply z(t), (previously denoted as F(t)), must respect:

$$\max(Re(\lambda)) < 0 \tag{21}$$

For the second and third approaches where the parameters of the model are assumed unknown, results are presented for three different levels of noise, where the SNR ranges from 0.25 to 10 and the algorithm's performance is evaluated after a fraction of the data has been processed, as well as after the whole data. Each of the 500 Monte-Carlo runs falls into one of 8 bins that characterize the strength of the evidence for model 1 vs model 2, according to the final probability attributed to each by the algorithm as expressed in Table 2.

Evidence	Probability of model 1
Very strong 1	[0.99, 1]
Strong 1	[0.95, 0.99[
Positive 1	[0.75, 0.95[
Weak 1	[0.5, 0.75[

Table 2. Evidence Labels

3.1.4. Influence of the input characteristics

The input signals in all of the previous simulations are fixed and periodic. Performing the same Monte-Carlo simulations described in the previous section, but varying the two parameters (period and duty cycle) of the input signal to the first brain area, one can try to determine how they influence the accuracy of the algorithm. The classification of the algorithm for each set of input parameters is scored according to the following formula:

$$S = \#(P(X) > 0.75) - \#(P(X) < 0.25) \tag{22}$$

3.1.5. Unknown parameters - covering the parameter space

This third approach generates the data exactly in the same way as the second one, but differs in the algorithm used to select the models. It does not have a one-to-one correspondence between models in the scenario and KFs in the MMKF. Instead, for a given model, it generates all the possible models where each parameter can take two values (partitionining the space in three equal parts) hence a model with n connections[1] generates 2^n different representations in the MMKF (minus the representations which are unstable).

This allows for a much better covering of the parameter space, hence increasing the likelihood of the MMKF converging to one of the KFs that correspond to the correct connectivity structure. In this case, 200 Monte-Carlo simulations are done.

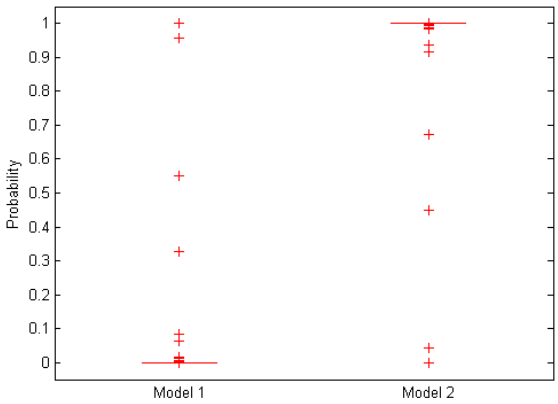

Fig. 5. Box plots of the posterior probabilities for each of the models in the intrinsic selection where the correct model is model 2

3.2. Results and Discussion

3.2.1. Simulations with known parameters

It is clear from Figure 5 that in almost all cases, model 2 ended up with probability 1, which leads to an unusual box plot. In the end, only 3 out of the 100 simulations had model 1 with a higher probability, and in 91 of the simulations, model 2 had a probability higher than 99%.

3.2.2. Simulations with unknown parameters

This second approach, closer to reality, exposes some of the weaknesses of the algorithm. When data are generated from model 1, the results in figure 6(a) seem close to perfect regardless of the SNR. However, when data are generated from model 2, figure 6(b) still reports that model 1 is widely preferred, which is incorrect.

This may mean that, since the parameters used to represent the models do not cover the parameter space adequately, not only does data from the structure of model 1 fit those parameters, but also data generated by model 2 will fit them in most cases. In the end, at the highest SNR and using the

[1] remember that in this context each connection in a model corresponds to a parameter

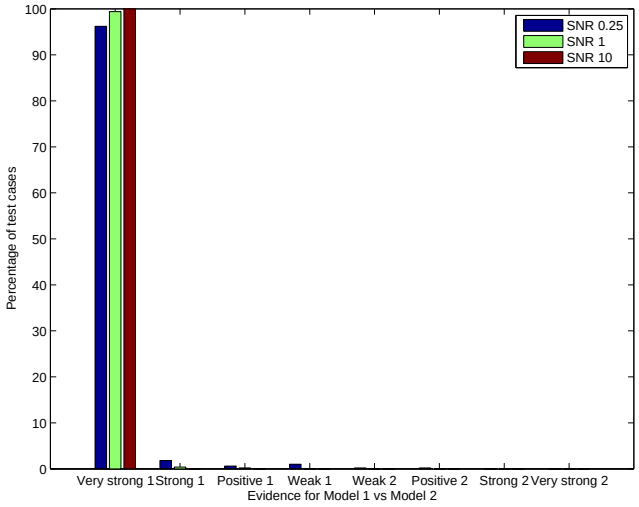

(a)

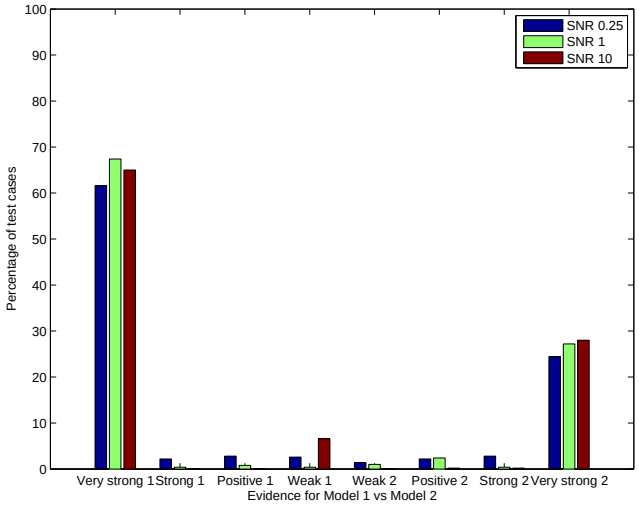

(b)

Fig. 6. Bar plots of the evidence for each model after 200s of data when the correct is (a) 1 or (b) 2

whole data, the second approach returns at least strong evidence for the correct model 64% of the time, and strong evidence for the wrong model 32.5% of the time.

3.2.3. Dependence on input

Figure 7 depicts the performance of this approach when model 1 generates the data, depending on the input parameters. It is clear that the parameters chosen initially are close to the peak performance of the algorithm for this data, which shows a tendency to decrease as the period of the input signal is diminished.

In general it should be possible to perform similar *a priori* studies to determine optimal input characteristics that maximize distinguishability of different connectivity models. In

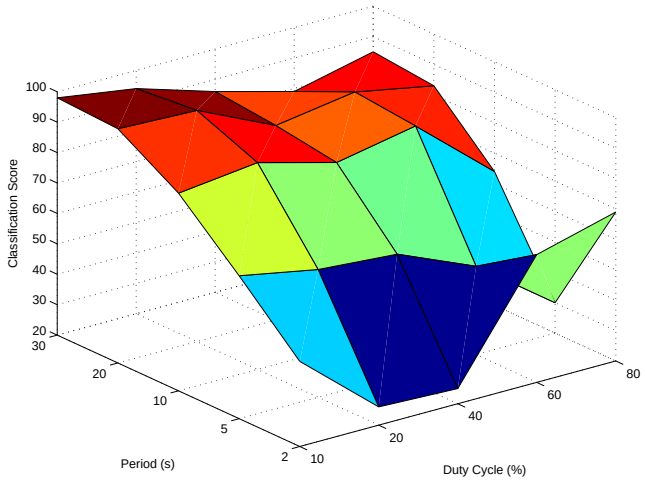

Fig. 7. Classification score for different input characteristics

practice, there has been some work on how to determine the effect of experimental designs on activity detection or HRF estimation using fMRI [24] and how to optimize these parameters [25]. Recently, there has been some work on the distinguishability of different HRFs in the framework of multiple-model SVOs [26].

3.2.4. Simulations with unknown parameters - covering the parameter space

The third approach consists of a classification task as hard as the one in the second approach (thus more realistic than the first one) but the algorithm is slightly modified in the expectation that it can overcome the weaknesses of the last approach.

By partitioning the parameter space, it is more likely that one of the KF in the MMKF will be *close* to the model generating the data, hence theoretically making the algorithm more robust and more capable of choosing correctly between different connectivity structures.

The results in figure 8(a) relative to data generated by model 1 are worse than the ones obtained by the second approach, but still particularly good especially with the whole data and SNR=10. On the other hand, for data generated by model 2 in figure 8(b), the algorithm now behaves correctly, as opposed to what happened in the second approach. Again, the classification accuracy increases with the SNR. Notably, with SNR=10 and using the whole data, this approach returns at least strong evidence for the correct model 91.5% of the time, which is strikingly better than the results of the previous approach.

3.2.5. Summary of the results for unknown parameters

In table 3 one can observe the results for unknown parameters with both algorithms (obtained using (22)). The lower scores for the single parameter algorithm are due to its consistent

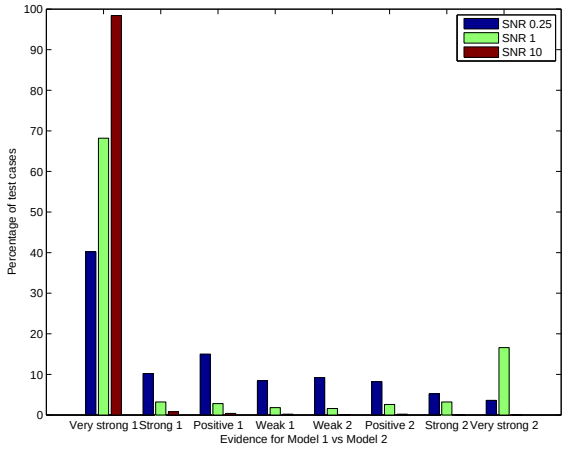

(a)

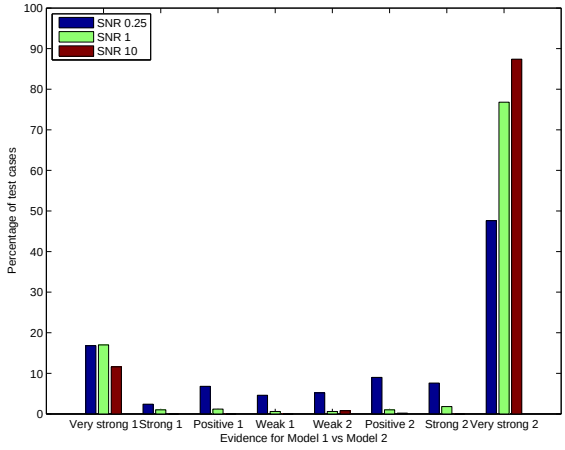

(b)

Fig. 8. Bar plots of the evidence for each model, with parameter space covering, after 200s of data when the correct is (a) 1 or (b) 2

selection of model 1 when model 2 is the correct one, and the SNR doesn't affect its score. For the algorithm that uses more than one filter per model thus covering the parameter space, the results are much better and the SNR impacts them directly.

4. CONCLUSION

In this work, the problem of estimating effective connectivity from fMRI data in the framework of DCM was tackled by using MMKFs.

First, the problem of estimating the HRF had to be addressed. Bilinearization and discretization were required to make it suitable for the MMKF. Given a set of different HRF models, the algorithm succeeds in picking the correct one and it can also be applied to empirical data after pre-processing.

The underlying DCM structure also needs to be discretized and then coupled with the HRF in a global state that represents the whole system. The algorithm performs very well when distinguishing between parametrized models.

	SNR		
	0.25	1	10
Single parameter	30.6	30.7	31.7
Parameter Covering	56	74.25	83.5

Table 3. Performance score (normalized to 100)

When the parameters are unknown (the case where the connectivity is tested), the algorithm performs poorly when using a single KF to represent a connecitivity structure, but its results are markedly better when several KFs are used for each connectivity structure.

In summary, a new approach for the estimation of neural connectivity from fMRI based on models (DCM) is proposed using multipled-model estimation techniques (MMKF) that may be more robust to the multi-modality of the posterior probabilities of the parameters than the classical technique.

4.1. Future Work

A comparison with DCM variational estimation followed by bayesian model selection is required to identify further weaknesses/strengths of the algorithm. Several points need to be addressed in the current form of the algorithm, such as the estimation of SNR, making it robust to temporal scaling in the DCM and amplitude of the signals. A practical way of applying the algorithm without knowledge of the HRF for each area must also be developed. Finally, finding automatic techniques to design the optimal input for a given connectivity distinction would also have interesting applications.

5. REFERENCES

[1] Barry Horwitz, "The elusive concept of brain connectivity.," *NeuroImage*, vol. 19, no. 2 Pt 1, pp. 466–470, 2003.

[2] S.R. Cajal, *Les nouvelles idées sur la structure du système nerveux chez l'homme et chez les vertébrés*, C. Reinwald, 1894.

[3] Olaf Sporns, Giulio Tononi, and Rolf Kötter, "The human connectome: A structural description of the human brain," *PLoS Comput Biol*, vol. 1, no. 4, pp. e42, 09 2005.

[4] P.A. Valdes-Sosa, A. Roebroeck, J. Daunizeau, and K. Friston, "Effective connectivity: Influence, causality and biophysical modeling," *NeuroImage*, 2011.

[5] Alard Roebroeck, Elia Formisano, and Rainer Goebel, "Mapping directed influence over the brain using

Granger causality and fMRI.," *NeuroImage*, vol. 25, no. 1, pp. 230–242, Mar. 2005.

[6] K.J. Friston, L. Harrison, and W.D. Penny, "Dynamic Causal Modelling," *NeuroImage*, vol. 19, no. 4, pp. 1273–1302, 2003.

[7] K.J. Friston, A. Mechelli, R. Turner, and C.J. Price, "Nonlinear responses in fMRI: The Balloon model, Volterra kernels and other hemodynamics," *NeuroImage*, vol. 12, pp. 466–477, 2000.

[8] J.J. Riera, J. Watanabe, I. Kazuki, M. Naoki, E. Aubert, T. Ozaki, and R. Kawashima, "A state-space model of the hemodynamic approach: nonlinear filtering of bold signals," *NeuroImage*, vol. 21, no. 2, pp. 547–567, 2004.

[9] L.A. Johnston, E. Duff, I. Mareels, and G.F. Egan, "Nonlinear estimation of the bold signal," *NeuroImage*, vol. 40, no. 2, pp. 504–514, 2008.

[10] H. Zhenghui, Z. Xiaohu, L. Huafeng, and S. Pengcheng, "Nonlinear analysis of the bold signal," *EURASIP Journal on Advances in Signal Processing*, vol. 2009, 2009.

[11] C. Silvestre, P. Figueiredo, and P. Rosa, "Multiple-model set-valued observers: A new tool for hrf model selection in fmri," in *Engineering in Medicine and Biology Society (EMBC), 2010 Annual International Conference of the IEEE*. IEEE, 2010, pp. 5704–5707.

[12] K. Friston, J. Mattout, N. Trujillo-Barreto, J. Ashburner, and W. Penny, "Variational free energy and the laplace approximation," *NeuroImage*, vol. 34, no. 1, pp. 220–234, 2007.

[13] J. Daunizeau, O. David, and KE Stephan, "Dynamic causal modelling: a critical review of the biophysical and statistical foundations," *Neuroimage*, 2009.

[14] M. Athans and P.L. Falb, *Optimal control: an introduction to the theory and its applications*, McGraw-Hill New York, 1966.

[15] R. Murray-Smith and T.A. Johansen, Eds., *Multiple Model Approaches to Modelling and Control*, Taylor and Francis systems and control book series. Taylor and Francis, London, UK, 1997.

[16] Rudolph Emil Kalman, "A new approach to linear filtering and prediction problems," *Transactions of the ASME–Journal of Basic Engineering*, vol. 82, no. Series D, pp. 35–45, 1960.

[17] Paulo Rosa, *Multiple-Model Adaptive Control of Uncertain LPV Systems*, Ph.D. thesis, Instituto Superior Técnico - Universidade Técnica de Lisboa, Portugal.

[18] D. Magill, "Optimal adaptive estimation of sampled stochastic processes," *Automatic Control, IEEE Transactions on*, vol. 10, no. 4, pp. 434–439, 1965.

[19] D. Lainiotis, "Optimal adaptive estimation: Structure and parameter adaption," *Automatic Control, IEEE Transactions on*, vol. 16, no. 2, pp. 160–170, 1971.

[20] Y. Baram and N. Sandell, "An information theoretic approach to dynamical systems modeling and identification," *IEEE Trans. on Automatic Control*, vol. 23, no. 1, pp. 61–66, feb 1978.

[21] Thomas Deneux and Olivier Faugeras, "Using nonlinear models in fMRI data analysis: Model selection and activation detection," *NeuroImage*, vol. 32, no. 4, pp. 1669–1689, Oct. 2006.

[22] J.W. Cooley and J.W. Tukey, "An algorithm for the machine calculation of complex fourier series," *Math. Comput*, vol. 19, no. 90, pp. 297–301, 1965.

[23] W. D. Penny, K. E. Stephan, Penny Stephan Mechelli, and K. J. Friston, "Comparing dynamic causal models," *Neuroimage*, vol. 22, pp. 1157–1172, 2004.

[24] A. Mechelli, C.J. Price, R.N.A. Henson, and K.J. Friston, "Estimating efficiency a priori: a comparison of blocked and randomized designs," *Neuroimage*, vol. 18, no. 3, pp. 798–805, 2003.

[25] T.D. Wager and T.E. Nichols, "Optimization of experimental design in fmri: a general framework using a genetic algorithm," *Neuroimage*, vol. 18, no. 2, pp. 293–309, 2003.

[26] C. Silvestre, P. Figueiredo, and P. Rosa, "On the distinguishability of hrf models in fmri," in *Engineering in Medicine and Biology Society (EMBC), 2010 Annual International Conference of the IEEE*. IEEE, 2010, pp. 5677–5680.